POLAR: Passive object localization with IEEE 802.11ad using phased antenna arrays

Dolores Garcia[†⋆], Jesus Omar Lacruz[†], Pablo Jiménez Mateo[†⋆], Joerg Widmer[†]

[†] IMDEA Networks Institute, Madrid, Spain

[⋆] Universidad Carlos III de Madrid, Madrid, Spain

E-mails: [†]{firstname.lastname}@imdea.org

***Abstract*—Millimeter-wave systems not only provide high data rates and low latency, but the very large bandwidth also allows for highly accurate environment sensing. Such properties are extremely useful for smart factory scenarios. At the same time, reusing existing communication links for passive object localization is significantly more challenging than radar-based approaches due to the sparsity of the millimeter-wave multi-path environment and the weakness of the reflected paths compared to the line-of-sight path.**

In this paper, we explore the passive object localization accuracy that can be achieved with IEEE 802.11ad devices. We use commercial Access Points (APs) whereas the station design is based on a full-bandwidth 802.11ad compatible FPGA-based platform with a phased antenna array. The stations exploit the preamble of the beam training packets of the APs to obtain Channel Impulse Response (CIR) measurements for all antenna patterns. With this, we determine distance and angle information for the different multi-path components in the environment to passively localize a mobile object. We evaluate our system with multiple APs and a moving robot with a metallic surface. Our system operates in real-time and achieves 6.5cm mean error accuracy and sub-meter accuracy in 100% of the cases.

***Index Terms*—Passive localization, IEEE 802.11ad, millimeter-wave (mm-wave) communications, phased antenna arrays**

I. Introduction

Industry 4.0 will transform the manufacturing and retail industry, requiring high-speed real-time information acquisition and massive data exchange between numerous devices and multiple central controllers [1]. Thanks to its high data rate, low latency and low susceptibility to interference due to the highly directional antennas, millimeter-wave (mm-wave) communications will be an important technology to enable automation and connectivity in future factories. At the same time, real-time tracking of moving objects (robots, mobile machines, etc.) is an important feature for factory automation that should, however, not interfere with the normal operation of the plant. Given the large bandwidth of mm-wave bands, integrating mm-wave communications and passive localization is an extremely promising approach to design accurate, scalable, low cost and ubiquitous passive tracking systems. Unlike approaches using a laser [2] which require an additional platform and resources, a wireless tracking system can be integrated with mm-wave communication at zero cost.

Passive tracking has been widely studied for lower frequencies [3–6]. These systems can achieve good accuracy due to the rich multi-path environment and low attenuation of the reflected paths as well as the increases in bandwidth and higher-order MIMO-capabilities of newer communication standards. While mm-wave systems can potentially increase location accuracy given the high bandwidth and thus time resolution of the channel compared to sub-6 GHz systems, building a sensing system at mm-wave frequencies is significantly more challenging. To overcome the high path loss in the mm-wave band, devices use phased-array antennas together with beamforming techniques for directional communication. The multi-path environment is sparse and the existing reflection paths are often weak or do not even reach a receiver. At the same time, the beam patterns of such phased arrays have many significant side-lobes [7]. While this is acceptable for communication, whenever a side-lobe illuminates the strong Line-of-Sight (LOS) path, weak reflections are often no longer detectable even when the pattern's main lobe is pointing towards that reflected path.

Prior work shows that mm-wave frequencies can provide sub-decimeter accuracy [8–10], but these systems are based on radar, without offering a communication link, where the aforementioned challenge of detecting reflections in the presence of a LOS path is not a problem. While a feasible solution, in the interest of cost and complexity it is much more promising to have a single mm-wave system for both communication and localization. Also, systems for joint communication and radar have been proposed [11–14], but they require simultaneous transmission and reception as well as very good self-interference cancellation capabilities not supported by current mm-wave communication devices. Other works use much more directional horn antennas [15], as then the impact of the LOS path is reduced, resulting in stronger reflections. However, to avoid moving parts and for rapid beam steering and switching between links, such fixed horn antennas will only be used in (static) niche scenarios and most commercial communication devices will use phased array antennas.

In this paper, we explore the accuracy of mm-wave passive location systems that can be achieved despite the aforementioned challenges. To this end, we design POLAR, a passive object localization system, which leverages Channel Impulse Response (CIR) information extracted from the preambles of beacon frames. Such beacon frames are sent by an Access Point (AP) via each of its available beam patterns to carry out

periodic beam training – the so-called Sector Level Sweep (SLS) – and thus maintain alignment of device's antenna beams for communication. The CIR is measured at the stations by means of correlating the incoming signal with repetitions of complementary Golay sequences of the preamble of IEEE 802.11ad frames. By analyzing CIR measurements over the multiple beacons corresponding to different beam patterns of a single SLS, we can estimate Angle of Departure (AoD) and time-of-flight of the different multi-path components visible at a given station. We further obtain the different amplifications each beam pattern causes on a given path.

Tracking changes of the CIR over time allows classifying reflections into static and mobile ones. This is a challenging task as some beam patterns may have a low amplitude in the direction of the reflection, or reflections themselves may be so weak as to be close to the noise floor in the CIR. However, the number of beam patterns in the SLS is typically large enough so that at least a few of the patterns provide a sufficiently good signal to be able to compare the different path amplifications due to the beam pattern shapes and thus determine angle information of the moving object. The SLS in the IEEE 802.11ad has a duration of around 1ms and happens every 102 ms [16], allowing for continuous location data acquisition at a sub-second level. The system does require a sufficiently strong reflector such as the smooth metallic surfaces that are very common in industrial factory settings. In contrast, detecting humans would be extremely challenging due to the low and irregular reflectivity of clothing. A single AP-station pair only provides very limited coverage given the constraints of planar phased arrays. Full coverage therefore requires multiple APs and stations, as is typical for mm-wave deployments. To evaluate our system, we implement a full-bandwidth receiver for standard-compliant 802.11ad frames on a large FPGA-platform to which we connect a phased antenna array. For the APs we use Commercial-Off-The-Shelf (COTS) 60 GHz devices. We study the performance of the proposed approach in an extensive measurement campaign.

Our paper makes the following contributions:

- We design and implement POLAR, a passive mm-wave location system for IEEE 802.11ad devices with zero overhead, that neither requires modifications to the beam training procedure nor the frame structure.
- We design a full-bandwidth FPGA-based testbed which is able to receive, detect and decode IEEE 802.11ad standard-compliant frames.
- We perform real-time indoor experiments tracking a moving robot using COTS 60 GHz APs together FPGA-based client stations. We show that the system achieves 17.6 cm mean accuracy, 6.5 cm mean accuracy with trajectory filtering, and sub-meter accuracy in 100% of the cases.

The paper is organized as follows. In Section II we explain the intuition behind our algorithm and the signal processing involved in the implementation of POLAR. Next, we present our testbed platform used to validate POLAR in Section III. The evaluation results for the proposed scheme are presented in Section IV. We survey related work in Section V and finally give concluding remarks in Section VI.

II. Passive Location System

Before presenting the details of POLAR, we first introduce some necessary background related to the beam training and physical layer of the IEEE 802.11ad standard.

A. IEEE 802.11ad background

1) Sector Level Sweep (SLS): COTS devices commonly use analog beam forming, where different phase shifts forming an Antenna Wave Vector (AWV) are applied to the antenna elements. This creates a set of directional beam patterns pointing in different directions, called a codebook. Which pattern from the codebook to select is determined by the beam training mechanism SLS, which is used to periodically (re-)align the antennas beams.

SLS, as used by current 802.11ad devices, works as follows. i) The AP transmits one beacon per sector, whila station listens using a quasi-omnidirectional beam pattern. ii) The roles are reversed, the AP listens with a quasi-omnidirectional beam pattern while the station sends a probe on each sector. iii) The AP and the station exchange the beam information and start transmitting directionally via the best transmit-receive sector pair. Some of the beam patterns used to send the probes will illuminate the object with different amplitudes while the angle of the reflection remains static over the short duration ($\sim$ 1ms) of a single SLS. We then exploit knowledge of the shape of the beam patterns to determine angle information.

2) Frame structure: Both the AP and the station use short IEEE 802.11ad control frames during the SLS phase [16]. The frame structure consists of a Short Training Field (STF) and a Channel Estimation Field (CEF), which form the preamble, header, data blocks and an optional beam forming training field, as shown in Fig. 1. This general structure is shared by all packet types.

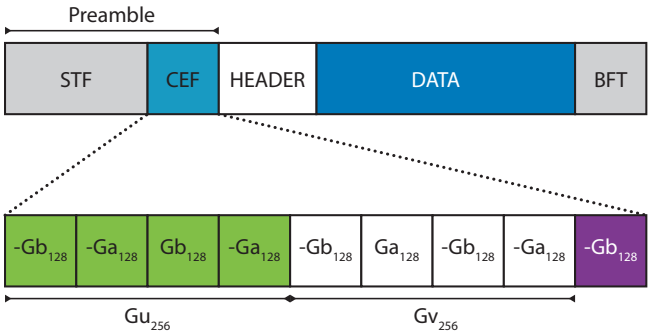

Fig. 1: General structure of IEEE 802.11ad packets with detailed Channel Estimation Field for control frames

The STF is used to perform frame detection, symbol synchronization, and Carrier Frequency Offset (CFO) estimation and compensation. The STF of a control frame is composed of 48 repetitions of 128-sample Golay sequences, Gb_{128}, followed by a single repetition of $-Gb_{128}$ and $-Ga_{128}$. The

CEF consist of 512-sample sequences, Gu_{512}, Gv_{512} followed by Gb_{128}, as detailed in Fig. 1. These sample sequences are composed of combinations of complementary pairs Ga_{128} and Gb_{128}, which make them suitable for CIR estimation thanks to their auto-correlation properties, as discussed next.

3) Golay sequence aided CIR estimation: The CIR is computed, as presented in [17], by taking advantage of the auto-correlation properties of complementary Golay sequences. The sum of the auto-correlation of a pair of complementary Golay sequences Ga_N and Gb_N of length N gives the delta function $\delta[n]$ which makes it suitable for multi-path detection in noisy environments. The CIR for each pair of complementary Golay sequences d is given by:

$$h_{G,d}[i] = \frac{1}{N}\sum_{n=0}^{N-1} r_{CEF}[i+n] \times \text{G}_N^*[n] \quad \forall\ d = 1, ..., D \tag{1}$$

r_{CEF} is the CEF field of the received frame, D is the number of repetitions of Golay sequences in the CEF and $\{\cdot\}^*$ is the complex conjugate operator. We use (1) to determine $h_{Ga,d}$ and $h_{Gb,d}$ for Ga and Gb, respectively. Finally, the estimated CIR is obtained by adding and averaging individual $h_{\text{Ga},d}$ and $h_{\text{Gb},d}$ results from (1), considering that $D = 4$ for the CEF structure from IEEE 802.11ad frames.

$$\mathbf{h}_{est} = \frac{1}{D}\sum_{d=1}^{D}(\mathbf{h}_{\text{Ga},d} + \mathbf{h}_{\text{Gb},d}) \tag{2}$$

The peaks in the CIR over the time domain correspond to the different multi-path components. Their amplitudes depend on the beam pattern being used and the reflection coefficient of the object. Not all beam patterns will include all paths in their CIR, as some directions may have a too low gain. An example of the CIR for two beam patterns is shown in Fig. 2(b), where the highest peak corresponds to the direct LOS path and the remaining ones correspond to reflections.

B. POLAR algorithm

The intuition behind our POLAR algorithm is as follows. We assume multiple APs in an indoor industrial area, where mm-wave deployments are envisioned to be dense. The CIRs is computed at the stations for each of the received frames. Note that COTS devices already do this in any case and this information would only have to be passed up to the driver level. Once a robot starts moving within the room, changes in the position (and orientation) of the robot translate into changes in the CIR. By analyzing the changes in the reflection patterns from the CIRs, we can determine delay and angle information of reflections which are then used to estimate the location of the moving robot.

For the measurements of an SLS, we develop a decision algorithm that allows us to consider only useful frames that do show changes in the CIR. This allows us to discard most of the data until a relevant reflection is detected, significantly reducing the overhead of the algorithm and the detection time, which is crucial for industry scenarios. No coordinating feedback between stations and APs is required and our passive location system is only based on information already available from the mm-wave physical layer. Good coverage in a small scenario is achieved with only 2 APs whereas a large room requires 4 APs, as will be shown in the evaluation section.

As a first step, our location system converts CIR measurements into Time of Arrival (ToA) at each station. Our algorithm localizes the moving object in 2D space. The quasi-optical behavior of the mm-wave channel implies that the energy received at a given station has reached it via a limited number of propagation paths. We denote by L the number of relevant paths. The downlink channel matrix towards a station C is given by

$$H = \sum_{l=1}^{L} \alpha_l s_C(v_l) s_a(\psi_l)^H, \tag{3}$$

where the superscript H denotes the conjugate-transpose, α_l is the complex power gain of a path l (which includes path loss and phase shift), and v_l and ψ_l are the unitary vectors that define the direction of arrival at the station and the direction of departure from the AP for the lth path, respectively. Finally, $s_C(v_l)$ and $s_a(\psi_l)$ are the steering vectors of the antenna arrays for station and AP for directions v_l and ψ_l, respectively.

The CIR that is obtained at the station depends on the beam pattern p active at the AP. Therefore, the channel observed by station C is

$$h_C = \sum_{l=1}^{L} \alpha_l s_C(v_l) s_a(\psi_l)^H p \tag{4}$$

More specifically, the CIR measured at station C is

$$h_{C,m}(t) = \sum_{l=1}^{L} \alpha_l p_m(\psi_l)\delta_{t-\tau_l} e^{i\phi_l} = \sum_{l=1}^{L} \beta_{l,m}\delta_{t-\tau_l} e^{i\phi_l} \tag{5}$$

where m is the beam pattern index. We define the scalar value $\beta_l = \alpha_l p_m(\psi_l)$ as the power received from each path and τ_l and ϕ_l are the delay and phase of the path l, respectively. Each path is amplified differently for each beam pattern. We use this fact to obtain the angle information as explained in the next section.

C. Angle of departure estimation

During beaconing, an AP changes through all of its available beam patterns. Whenever an AP performs an SLS, the station captures the preamble and obtains the CIR corresponding to the different beam patterns using (1) and (2), as shown in Fig. 2. As a first step, our algorithm converts the CIR information into directions of departure of the reflections θ_l.

For this, it is necessary to first determine the peak which corresponds to the reflection of the object. Because of the large bandwidth of mm-wave, the CIR can resolve the different multi-path components p_l captured by the receiver. During the motion of the object in the environment, some of these multi-path components will remain stationary while others will appear, disappear, or change. Let $H = |h(t)_{C,m}|$ denote the magnitude of the calculated CIR. We define $H_{S,m}$ as the

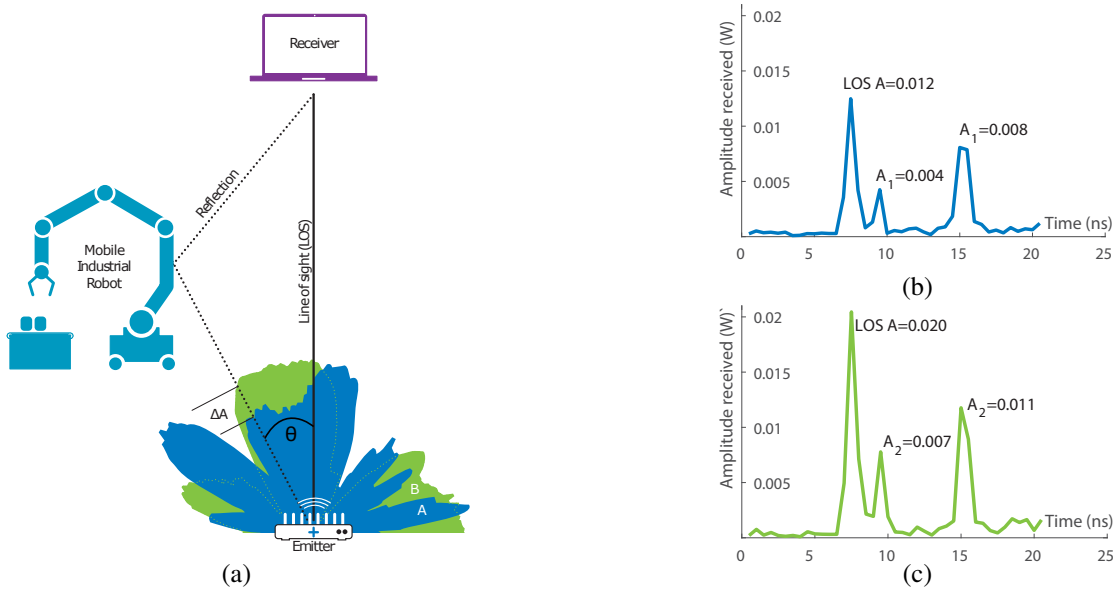

Fig. 2: (a) Intuition behind the POLAR algorithm, where different beam patterns amplify the same path with different gains. (b) Calculated CIR from beam pattern A, with less gain in the object direction, (c) Calculated CIR for beam pattern B, showing higher amplification for the reflection from the object.

stationary components and $H_{M,m}$ as the mobile ones for a given beam pattern m, where $H_{S,m}$ is obtained taking the empty room as a reference. It is possible that certain reflections are not observed for all beam patterns, as the beams cover different areas. Therefore, we estimate whether a certain frame shows a non-stationary reflection. For this we define

$$\phi_{A,M,m}(k) = \int_{1+kw-kO}^{1+(k+1)w-kO} H_{M,m}(\tau)d\tau \tag{6}$$

where the integral is calculated with the trapezoidal approximation, w is the window of the segmentation and O is the overlap between segments, so that the cluster structure is preserved [18].

We define the correlation between the smoothed CIR as

$$S_{M,S,m} = < \frac{\phi_{A,M,m}}{\|\phi_{A,M,m}\|}, \frac{\phi_{A,S,m}}{\|\phi_{A,S,m}\|} > \ . \tag{7}$$

The binary result for a reflection is obtained by setting a similarity threshold to the correlation function

$$\chi_i = \begin{cases} 0 & \text{if } S_{M,S,m} > \kappa, \\ 1 & \text{if otherwise} \end{cases}$$

where κ is the chosen threshold value. This method allows us to only check frames for which $\chi_n = 1$, i.e., a reflection from an object is estimated with high probability. This reduction of frames translates into a lower computation time. In addition, the accuracy of the estimated ToA is higher as no false peaks are detected. We compare the CIR measurements for a given beam pattern i, and define the difference function $D_i(t)$

$$D_n(t) = H_{M,i}(t) - H_{S,i}(t) = \sum_{l=1}^{L_M} \beta_{M,l,i}\delta_{t-\tau_l} - \sum_{l=1}^{L_S} \beta_{S,l,i}\delta_{t-\tau'_l}. \tag{8}$$

With the above definitions, we use Algorithm 1 to detect K new reflections, with arrival times $t_1, .., t_K$. We define $R_{M,S,i} = E\left\{H_{M,i}(t+z)H^*_{S,i}(z)\right\}$, and R is taken as the reference time of arrival of the LOS path for all CIR measurements. Offsets are corrected using the correlation function $R_{M,S}$. The *peaks* function estimates all local maxima in a vector of data and the *remove duplicates* function eliminates repeated elements of a vector. This method outperforms typical threshold models to detect new reflections as they are inexact in cases where the noise floor is high. Our algorithm also outperforms major peak removal models, that may not consider relevant peaks in case they are close to noise levels.

Once a new path has been observed, the AoD $\hat{\theta}$ of the path is estimated using the amplification a_m that the different beam patters introduce to the l^{th} path. The amplitude observed on the CIR of the l^{th} path P_l amplified by beam pattern m of the AP is $\beta_{l,m}$, as in (5). This can be observed in Fig. 2, where different beam patterns show different amplitudes for the same multi-path components.

We obtain $P_l = [p1, \ldots, p_N]$, the vector of powers of the path. Out of the 64 available beam patterns, we consider the N beam patterns with the highest measured Signal-to-Noise Ratio (SNR). Adding low SNR measurements to the estimation of the Angle of Arrival (AoA) would result in a less accurate overall estimation. We normalize $\frac{P_l}{\|P_l\|} = \frac{A_l}{\|A_l\|}$, where A_l is the vector of introduced amplitudes to the l^{th} path of the N beam patterns. Let $x_m(\theta)$ denote the amplification of the m^{th} beam pattern in direction θ, and $X_m = [x_m(\theta_1), \ldots, x_m(\theta_G)]$ be the shape of the m^{th} beam pattern. G denotes size of the grid of the measured beam patterns. Then $X = [X_1, \ldots, X_N]^T$ is the matrix with column i containing the measurement of $X_m(\theta_i)\ \forall m$.

Algorithm 1: Estimation of the K new paths

Data: $H_{M,n}$,$H_{S,n}$ $\forall n$ st. $\chi_n = 1$
Result: $[t_1, ...t_K]$, times of arrival of the new reflections.
initialization $n = 1$, R;
for $i = 2 : N$ **do**
  $\text{offset}_M = R - \max(R_{M,S,i})$
  $H_{M,i} = \text{circshift}(H_{M,i}, \text{offset}_M)$
  $\text{offset}_S = R - \max(R_{S,M,i})$
  $H_{S,i} = \text{circshift}(H_{S,i}, \text{offset}_S)$
end
for $i = 1 : N$ **do**
  $[t_{1,i}, ..t_{l,i}] = \text{peaks}(D_n(t))$
  $[t_1, ...t_K] = [t_1, ...t_K, t_{1,i}, ..t_{l,i}]$
  $[t_1, ...t_K] = \text{remove duplicates}([t_1, ...t_K])$
end

In order to obtain the NLoS AoD of path l, $\hat{\theta}_l$, that best matches the power measurements of the receiver, it remains to minimize the absolute error cost function:

$$\hat{\theta}_l = arg\min_{\theta} \sum_{i=1}^{G} \left(\frac{A_l}{\|A_l\|} - \frac{X(\theta_i)}{\|X(\theta_i)\|} \right) \tag{9}$$

D. CIR-based distance estimation

Using (9) we can now formulate the tracking algorithm. Since no phase information is assumed, and no time stamps are implemented, the distance information is obtained from the CIR measurements. We consider the CIR measurements in which the reflection is observable and obtain the difference of distance between the LOS path and the reflection as the difference of samples between the two peaks, t_{LOS} and $t_{\text{reflection}}$. Sampling is done every $\frac{1}{BW} = 0.56$ ns. Because of the cluster structure of the mm-wave channel [18], we can distinguish reflections separated by a minimum of two samples. Therefore, our algorithm has a resolution of 1.1 ns. With the previously calculated angle information, the distance from the detected object to the AP i, $D_{i,r}$ is obtained as:

$$D_{i,r} = \frac{(d_{i,j} + d_r)^2 - d_{i,j}^2}{2(d_{i,j} + d_r - d_{i,j}\cos(\hat{\theta})} \tag{10}$$

where $d_{i,j}$ is the (known) distance between AP_i and client j, $\hat{\theta}$ is the previously obtained angle and $d_r = t_{\text{reflection}} * \frac{1}{BW} * c$, where c is the speed of light and the bandwidth BW of our system is 1.79 GHz.

E. Multiple AP coverage

Mm-wave deployments will typically be dense, to overcome range limitations and blockage from obstacles, as well as limited antenna aperture. For our system, we use COTS devices with an angular range of $60°$, while the phased antenna array connected to the FPGA has an angular range of $120°$. While (limited) communication may be possible beyond those angles, the gains are typically to weak to detect reflections. Therefore, in order to ensure good location accuracy as well as coverage, our algorithm uses data from available APs and stations.

F. Kalman filter correction

Given that the object motion is typically smooth, we apply a forward Kalman filter to the trajectory. We consider the following mobility model

$$\begin{aligned} x_{t+1} &= x_t + w, \qquad w \sim \mathcal{N}(0, \sigma_e^2) \\ y_{t+1} &= x_{t+1} + v, \qquad v \sim \mathcal{N}(0, \sigma_m^2) \end{aligned} \tag{11}$$

where y_t is the measurement of location of the client at time t and x_t is the real location. This model corresponds to uniform linear motion with location error σ_m. The expected location is obtained by the following iterative model

$$\begin{aligned} x_{t+1} &= \left(\frac{1}{\sqrt{\sigma_{x_n}^2 + \sigma_e^2}} + \frac{1}{\sigma_m} \right)^{-1} \left(\frac{\bar{x}_n}{\sqrt{\sigma_{x_n}^2 + \sigma_e^2}} + \frac{y_{n+1}}{\sigma_m} \right) \\ \sigma_{x_{n+1}}^2 &= \left(\frac{1}{\sqrt{\sigma_{x_n}^2 + \sigma_e^2}} + \frac{1}{\sigma_m^2} \right)^{-1}. \end{aligned} \tag{12}$$

III. Implementation

Our practical implementation of the tracking system has the following parts.

A. Transmitter side

For the APs we use MikroTik wAP 60G routers. The IEEE 802.11ad compliant device uses a Qualcomm Atheros QCA6335 60GHz chipset with a planar phased antenna array of 6x6 elements. This device has an angular range of $60°$ and can achieve link distances of up to 200m. For the experimental evaluation, we use the preconfigured codebook of the router and the default firmware. We chose the MikroTik because of its high range and affordability make it suitable for industrial environments. In a typical mm-wave deployment, the limited angular range of the antenna requires that more than one AP will have to be placed to provide full room coverage. Newer devices, such as the MikroTik wAP 60Gx3 AP, already provide a set of three antennas that jointly cover $180°$, which simplifies deployments.

B. Receiver side

On the receiver side, we use a full-bandwidth FPGA-based baseband system connected to a Sivers 60 GHz RF development kit that integrates a 16+16 element phased antenna array together with 60 GHz up/down converters [19]. The system is capable of capturing and processing frames from any IEEE 802.11ad compliant device.

Although the testbed is capable of working as a transceiver, to perform the experiments conducted in this paper, we only exploit the receiver capabilities of the system. To this end, we develop AXI-stream IP blocks to be able to detect and process IEEE 802.11ad compliant frames at full-bandwidth

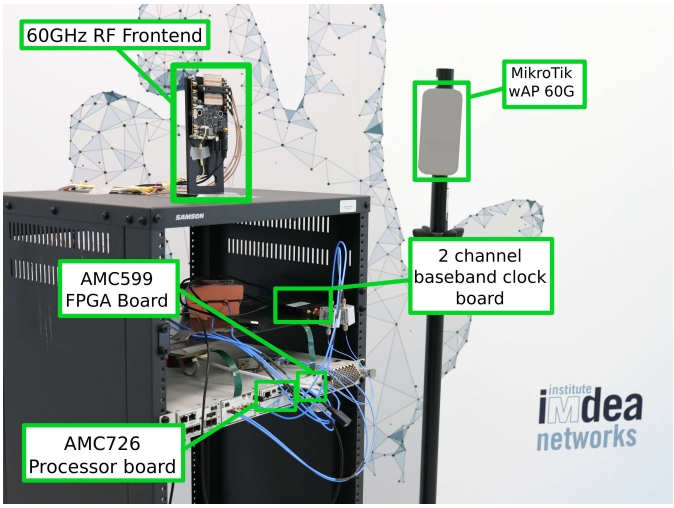

Fig. 3: Photo of the equipment used to implement POLAR

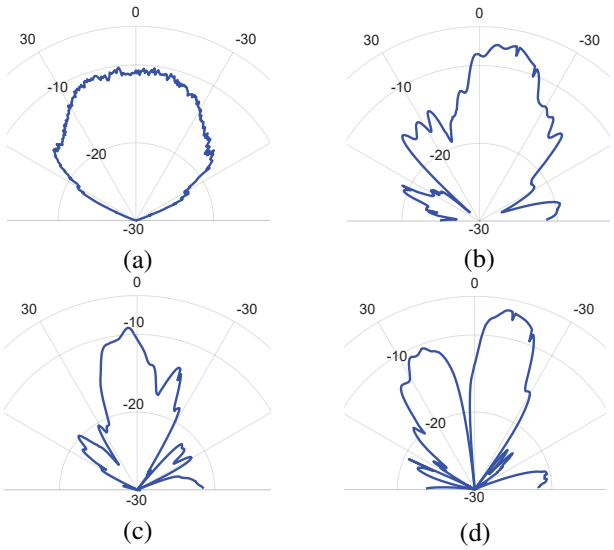

Fig. 4: (a) Measured quasi-omnidirectional receive beam pattern from the EVK06002 predefined codebook. Subfigures (b), (c) and (d) are examples of the transmit beam patterns from the predefined codebook of the MikroTik routers

and save them directly to the on-board DDR memory to be post-processed offline[1].

The RF front-end [20] is capable of working at 4 different 2.16 GHz wide IEEE 802.11ad channels and provides analog beam-forming capabilities using phase shifters with 6 bit resolution. The predefined codebook includes 64 different sectors (AWV). For the experiments conducted in this paper, we use a quasi-omnidirectional receive beam pattern from the predefined codebook. This is compliant with current COTS device behavior which only uses directional transmit beam patterns but quasi-omnidirectional reception. The measured radiation pattern is presented in Fig. 4(a).

The equipment used for the transmitter and receiver is shown in Fig. 3.

C. Beam pattern measurements

To obtain the shape of all the beam patterns of the transmitter used for beam training, we fix the router to a custom rotation table that steers mechanically over the different azimuth angles. We time the movement of the rotation table to wait for a full SLS before moving to the next angle. Our receiver [19] is placed at a distance of 5 m to the router and facing it at a zero degree angle. We record the Received Signal Strength (RSS) of the different beam patterns and then change the angle for the next measurement. The rotation table advances in steps of 1°, giving approximately one degree resolution in our angle estimation. Fig. 4(b), (c) and (d) show examples of the measured beam patterns. The irregularity of the beam patterns from the predefined codebook is helpful in that the correlation between the different beam patters is low, and therefore the amplifications are well determined.

[1]While the system is capable of real-time processing of the received IQ samples, for this paper we use the testbed in a mixed hardware-software design, where the preamble is processed in hardware while the rest is decoded offline using a software model.

IV. Evaluation

In this section we present results of our extensive measurement campaign to test POLAR over multiple configurations, changing the position of the AP, station and the trajectory. We aim to cover typical scenarios that can be found in an industrial setting. First, we describe the scenarios and then we present and analyze our results.

All the experiments are done in real-time. The experiments are set up in an empty room which is 6.2x23 m in size and has no furniture. While in this environment the reflections mainly come from the walls or the object, the system also works on more complex environments where fixtures provide additional static reflections. As a moving robot, we use a metal cylinder with 25 cm of diameter mounted on a moving platform.

A. Small scale scenario

The first simple baseline experiment consists of a longitudinal trajectory parallel to the line that connects the station and the AP, as shown in Fig. 5 (a). For this experiment, we use one AP and one station which are 5 m apart in the middle of the room. The reflector moves along the trajectory at a constant speed. This trajectory provides first insights into the angular resolution and coverage of a single AP and station pair. As can be seen in Fig. 5 (a), the accuracy of our system is very high as long as we remain within the aperture of the antenna array. Even though we use only one AP and one station the beam patterns of the MikroTik router perfectly cover such a trajectory with enough power and only fail to track the object for extreme angles at the station where the quasi-omnidirectional beam pattern only provides low antenna gain, as shown in Fig. 4 (a).

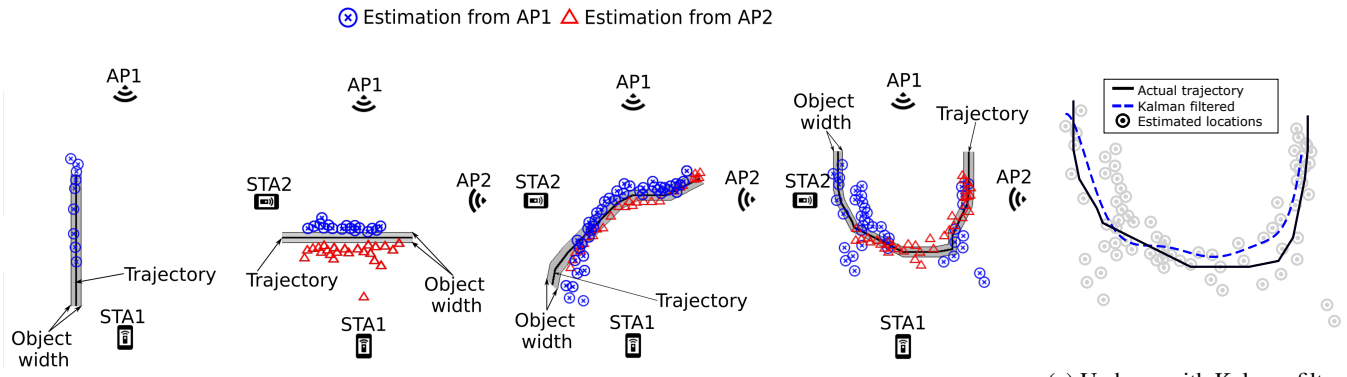

(a) Vertical trajectory (b) Horizontal trajectory (c) Diagonal trajectory (d) U-shaped trajectory (e) U-shape with Kalman filtering

Fig. 5: Experimental results for the small scale scenario

To test the robustness of our system, we perform another experiment with a transversal trajectory that crosses directly through the middle of the connection as seen in Fig. 5 (b). The most challenging tracking trajectories are those that cross the path between the AP and the station, and therefore have worse reflections than those parallel to the main link, since there are many points where the angle of the reflection is too steep for detection. Also, when crossing the line between the devices, the power of the signal drops significantly since the LOS path is blocked and there are usually no suitable reflections from the object that can be detected. Therefore, more than one AP and station is required to obtain sub-meter accuracy for arbitrary trajectories. We use 2 stations and 2 APs which provide sufficient coverage and, therefore, we are able to track the reflector as seen in Fig. 5(b).

After covering simple straight trajectories (that are nevertheless common in automated industry environments), we perform experiments with slightly more complex trajectories. For these trajectories, we use multiple APs to achieve coverage and accuracy. The realistic trajectories, due to the more organic movement, present a richer variety of angles to cover and more blockages by the reflector, thus making it harder to achieve sub-meter accuracy.

Fig. 5(c) shows the first of those experiments, the reflector crosses the middle of the environment in a diagonal path that crosses links AP1-Station1 and AP2-Station2. This trajectory mimics, for example, an autonomous robot that changes its direction to adapt to its surroundings. Fig. 5(c) shows the experimental setup and results. There are a few estimates that have a bias at the beginning of the trajectory due to the reflector being outside of the range of our system. However, for the rest of the trajectory, our system is capable of locating the moving object even in areas where there is no coverage by one of the APs.

Fig. 5(d) shows results for a U-shaped trajectory, which covers a larger area crossing the two links and getting very close to station 2. As a consequence, for many locations, only one AP can contribute to the localization of the reflector. This trajectory mimics again that of autonomous robots circumnavigating an obstacle on the floor. The first points of the trajectory, upper left, are only covered by AP1, and AP2 starts to contribute later in the trajectory. The bottom part is not covered by AP1 since the angle is too steep, but AP2 provides enough coverage there. The last section of the trajectory is covered by both APs simultaneously.

To show how the estimated points are used to determine a trajectory, Fig. 5 shows the raw estimates which are then used as input for the Kalman filter explained in Sec. II-F. Fig. 5e shows the result of applying such filter to the U-shaped scenario. Even in the presence of outliers as seen for the bottom left and bottom right points, the filter is robust enough to predict the trajectory of the reflector with very good accuracy.

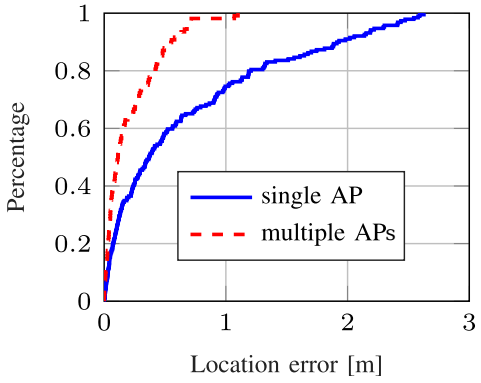

Fig. 6: CDF of the location error

Fig. 6 shows the performance of our system across all scenarios. The continuous line shows the location error when using only one AP. Even with one AP only, the error is less than one meter in 74% of the cases. When using multiple APs, 2 in our experiments, and a Kalman filter, the error is less than 1 meter in 98% of the cases, which shows the robustness of POLAR. These results can be further improved with custom beam patterns or a larger number of APs.

We further estimate how robust our location system is to SNR variations by fixing a position for the moving robot

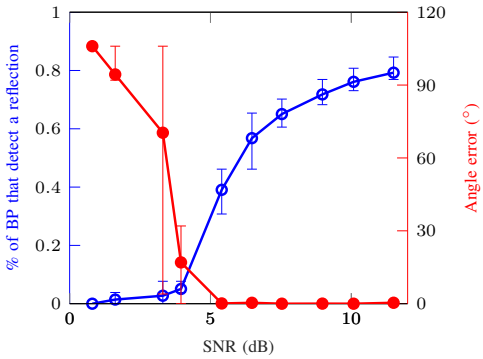

Fig. 7: Probability of detecting the reflection of the object with varying SNR.

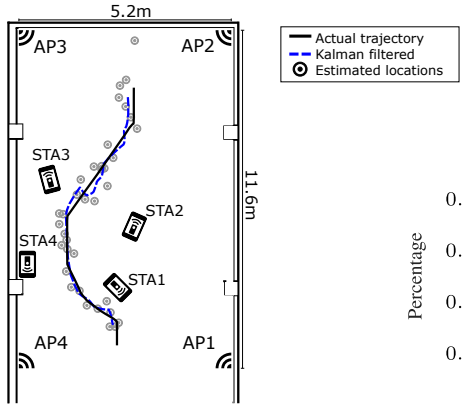

Fig. 8: Estimated trajectory with Kalman filtering and 4 APs.

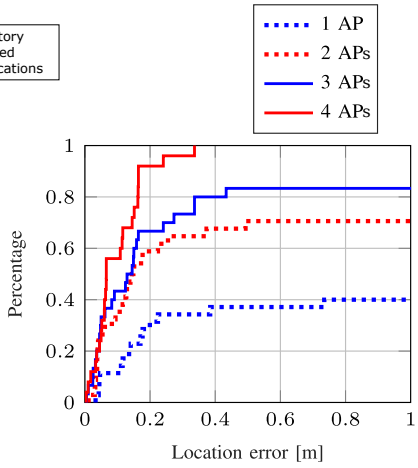

Fig. 9: CDF of the location error

and lowering the SNR on the receiver side by reducing the gain of the RF amplifiers. The results are presented in Fig. 7. As expected, the fraction of beam patterns that detect the reflection decreases with lower SNR, resulting in high angle errors for SNR values smaller than 4 dB. It is important to remark that even for low SNRs the reflection can still be detected reliably with POLAR, down to 6 dB. We also observe that the angle error for different SNR values behaves inversely to the probability of detection. Our experimental results show that detecting the reflection in a small number of beam patterns per beacon (around 10 to 15 out of 64) is sufficient for accurate angle estimation.

B. Large scale scenario

We next investigate a large scale scenario that covers the whole room. For this trajectory, we use up to 4 APs to achieve full room coverage. Fig. 8 shows the experimental set up and the raw estimated points which are inputs for the Kalman filter used to obtain a smoothed trajectory, also presented in the figure. Fig. 9 shows the performance of POLAR for this deployment considering different numbers of APs. The graph shows the location estimation error when using from one to four APs and when the data has been processed using the Kalman filter. When only one AP is used, the estimation error is low for the observed region of the trajectory, corresponding to about 30% of the whole trajectory, but stays constant after that, as the rest of the trajectory is not observed and thus has infinite location error. For the cases with two and three APs, we observe an increase in coverage and accuracy as a larger and larger region of the trajectory is covered by more links. For the scenario with 4 APs, the whole trajectory is covered and our algorithm achieves a mean error of 6.5 cm.

C. Limitations and challenges

POLAR is designed to use affordable COTS devices without any further modification. This has some limitations that are worth mentioning and that would not exist using custom hardware. The MikroTik APs that we use have an effective angular range of 60° (from −30° to 30°) which provides limited coverage. Also, the omnidirectional beam pattern that we use in our receiver only covers 120° (from around −60° to 60°), making it more difficult to capture all of the reflections. We did not modify the beam patterns of the MikroTik routers, and therefore we are limited by them. We also found that the routers provide better coverage at some angles that at others, making it easier to locate objects at certain angles. Further modifications and custom beam patterns of these devices would allow to achieve even better performance.

Another limitation is the object material. While flat reflective surfaces such as metal that are typically found in industry scenarios work very well, other materials such as cardboard or clothes worn by a human are much more challenging. The low and irregular reflectivity of clothing and the porous material of cardboard did not allow for sufficiently strong reflections to be detected reliably, constraining the use cases for which such passive localization mechanisms can be used.

V. Related Work

Passive location algorithms are a topic of increasing interest. In this section, we discuss several prior works in this area and highlight the differences to our passive localization algorithm.

A. Lower frequency sensing

There has been extensive work on lower frequency sensing systems [3–6, 21]. These systems achieve high accuracy due to the rich multi-path environment and strong reflections. General approaches for passive location estimation in lower frequencies rely on AoA and ToA estimation. The works in [3–6] all rely on CSI measurements for object location. Spotfy [4] makes use of AoA and ToA obtained from the CSI information. It critically relies on OFDM for the ToA estimation to be able to refine measurements over many different sub-carriers. The system achieves a 40 cm location error (for deployments of up to 55 AP, with 3 antennas for each AP). Md-track [3] improves over [4] and even achieves an accuracy of 0.36 cm, by successively iterating over estimates of AoA, ToA and

Doppler to enhance the multi-path resolution. This accuracy is achieved with 8 antennas and 40 MHz of bandwidth. These systems are MIMO systems with one RF chain per antenna, unlike mm-wave systems which use a phased array connected to a single RF chain. The latter makes channel estimation significantly harder and common multi-resolution algorithms such as MUSIC or ESPRIT cannot be used as the required per antenna information is not available. Also, current mm-wave systems are single carrier and cannot use OFDM-based ToA refinement. RSSI-based approaches have been proposed [21], but they achieve lower accuracy due to the coarse RSSI granularity.

B. Radar

Radar systems are often used for obstacle detection and human activity recognition as synchronization between transmitter and receiver clock allows for precise phase information [8, 9, 11]. Commercial 60GHz radar systems are readily available [8, 22] but requite custom hardware not designed for communication. These systems are designed to filter out the direct path component from transmit to receiver antenna and therefore do not suffer from the problem of weak reflections. This makes accurate location estimation much easier. The systems require full-duplex capabilities, which are, however, not yet available for current mm-wave communication systems. Among the state of the art, [11] uses the preamble structure of the 802.11ad standard to obtain the CIR and a threshold method to detect the reflections. It proposes a joint vehicular communication and radar system, but it does not address how to enable full-duplex mm-wave communications. In contrast, [9] uses a more classical approach, building a dedicated system of an analog FMCW radio front-end for object detection with a bandwidth of 1.79 GHz. The works [13, 23] propose multi-armed beam patterns to illuminate a higher number of directions at a time. Among the systems that achieve accurate location in a radar context is [9] that achieves decimeter level accuracy.

C. Mm-wave localization for beam training

There exist extensive research on active mm-wave location systems [24–26]. These works aim to localize users to achieve better beam training and AP associations, to establish communication links and predict handovers in case the link is about to fail. Therefore, the goal is to estimate the dominant path and not necessarily the entire multi-path environment. In [24], the authors use the CSI information obtained through a modification of the firmware of the router and calculate the AoA using a maximum likelihood approach. The work in [26] uses the CIR measurements to extract the LOS and correlates this against known beam patterns to obtain the AoA. We base our algorithm on the intuitions provided by these works on sparse channel estimation and sector information.

D. Mm-wave passive localization and multi-path estimation

There is little work studying passive localization for mm-wave communication and COTS devices, where receiver and transmitter are spatially separated. As discussed previously, it is indeed challenging to obtain good results given that reflections from objects are angle-dependent and often weak. Previous work on multi-path estimation applied to beam training and AP association, [23, 27], estimate the different multi-path components of the channel. However, the primary goal of these works is to determine the strong static reflections of the multi-path environment to use them for communication. In contrast, for passive localization the potentially weak reflections of the object are relevant. This is a significantly more challenging problem. To address it, some work has been presented using horn antennas [15, 28], which only focus the energy in one direction and do not suffer from side lobes. The LOS path is therefore not always present and the reflections are much easier to observe. [28] uses RSS to obtain an accurate estimation of heart rates, with 98.4% accuracy. The work in [15] is also based on RSS information, using a Vubiq and horn antennas with a rotating platform. Initially, the user location is obtained by scanning the room by brute force and movement is tracked over RSS changes. However, most consumer mm-wave devices use phased arrays instead of inflexible horn antennas, and we, therefore, base our system on the more phased array antennas.

To the best of our knowledge, no prior work has been presented that matches these constraints. Our work clearly differs from the above literature, as we present an object location system based on CIR measurements and compressed angle estimation obtained from the beam pattern shapes. Unlike other approaches, we design a system based on COTS devices and an FPGA system, both equipped with phased arrays and working with standard-compliant 802.11ad frames. This confirms that with our algorithm, object detection can be achieved with consumer equipment.

VI. Conclusions and future work

We designed and implemented a mm-wave passive tracking system using COTS IEEE 802.11ad APs together with an FPGA-based station. CIR measurements were obtained from the IEEE 802.11ad SLS to obtain angle and direction information of a moving robot. We show not only that it is possible to implement a joint communication and sensing system but also that it is possible to obtain sub-meter accuracy from weak reflections coming from the moving object. To overcome the hardware limitations, we use multiple APs to cover an entire room. Even higher accuracy could be achieved with hybrid antenna arrays for mm-wave systems, which are already included in the upcoming IEEE 802.11ay standard. Besides, we leave for future work the integration of second-order static multi-path components for environment mapping, which could be of high interest for connected factories.

Acknowledgment

This work was supported in part by the Region of Madrid through TAPIR-CM (S2018/TCS-4496) and PinPoint5G+ RTI2018-094313-B-I00 (MCIU/AEI/FEDER, UE).

REFERENCES

[1] B. Chen, J. Wan, L. Shu, P. Li, M. Mukherjee, and B. Yin, "Smart Factory of Industry 4.0: Key Technologies, Application Case, and Challenges," *IEEE Access*, vol. 6, pp. 6505–6519, 2018.

[2] Y.-S. Chou and J.-S. Liu, "A robotic indoor 3d mapping system using a 2d laser range finder mounted on a rotating four-bar linkage of a mobile platform," *International Journal of Advanced Robotic Systems*, vol. 10, no. 1, p. 45, 2013.

[3] Y. Xie, J. Xiong, M. Li, and K. Jamieson, "md-track: Leveraging multi-dimensionality in passive indoor wi-fi tracking," *CoRR*, vol. abs/1812.03103, 2018.

[4] M. Kotaru, K. Joshi, D. Bharadia, and S. Katti, "SpotFi: Decimeter Level Localization Using WiFi," in *Proceedings of the 2015 ACM Conference on Special Interest Group on Data Communication*. New York, NY, USA: ACM, 2015, pp. 269–282.

[5] B. Wei, W. Hu, M. Yang, and C. T. Chou, "From Real to Complex: Enhancing Radio-based Activity Recognition Using Complex-Valued CSI," *CoRR*, vol. abs/1804.09588, 2018.

[6] W. Wang, A. Liu, M. Shazad, K.Ling, and S. Lu, "Device-free Human Activity Recognition Using Commercial WiFi Devices," *IEEE Journal on Selected Areas in Communications*, vol. 35, p. 11181131, 2017.

[7] D. Steinmetzer, D. Wegemer, M. Schulz, J. Widmer, and M. Hollick, "Compressive Millimeter-Wave Sector Selection in Off-the-Shelf IEEE 802.11Ad Devices," in *Proceedings of the 13th International Conference on Emerging Networking EXperiments and Technologies*, ser. CoNEXT '17. New York, NY, USA: ACM, 2017, pp. 414–425.

[8] Texas Intruments. (2018, April) Traffic Monitoring Object Detection and Tracking Reference Design Using Single-Chip mmWave Radar Sensor. [Online]. Available: http://www.ti.com/lit/ug/tidud31a/tidud31a.pdf

[9] F. Adib, Z. Kabelac, D. Katabi, and R. C. Miller, "3D Tracking via Body Radio Reflections," in *11th USENIX Symposium on Networked Systems Design and Implementation (NSDI 14)*, Seattle, WA, 2014, pp. 317–329.

[10] J. Lien, N. Gillian, M. E. Karagozler, P. Amihood, C. Schwesig, E. Olson, H. Raja, and I. Poupyrev, "Soli: Ubiquitous Gesture Sensing with Millimeter Wave Radar," *ACM Trans. Graph.*, vol. 35, no. 4, pp. 142:1–142:19, Jul. 2016.

[11] P. Kumari, J. Choi, N. Gonzlez-Prelcic, and R. W. Heath, "IEEE 802.11ad-Based Radar: An Approach to Joint Vehicular Communication-Radar System," *IEEE Transactions on Vehicular Technology*, vol. 67, no. 4, pp. 3012–3027, April 2018.

[12] P. Kumari, N. Gonzalez-Prelcic, and R. W. Heath, "Investigating the IEEE 802.11ad Standard for Millimeter Wave Automotive Radar," in *2015 IEEE 82nd Vehicular Technology Conference (VTC2015-Fall)*, Sep. 2015, pp. 1–5.

[13] J. A. Zhang, X. Huang, Y. J. Guo, J. Yuan, and R. W. Heath, "Multibeam for Joint Communication and Radar Sensing Using Steerable Analog Antenna Arrays," *IEEE Transactions on Vehicular Technology*, vol. 68, no. 1, pp. 671–685, Jan 2019.

[14] L. Han and K. Wu, "Joint wireless communication and radar sensing systems - state of the art and future prospects," *IET Microwaves, Antennas Propagation*, vol. 7, no. 11, pp. 876–885, August 2013.

[15] Y. Zeng, P. H. Pathak, Z. Yang, and P. Mohapatra, "Human Tracking and Activity Monitoring Using 60 GHz mmWave: Poster Abstract," in *Proceedings of the 15th International Conference on Information Processing in Sensor Networks*, Piscataway, NJ, USA, 2016, pp. 25:1–25:2.

[16] IEEE 802.11 working group, "Wireless LAN Medium Access Control (MAC) and Physical Layer (PHY) Specifications Amendment 3: Enhancements for Very High Throughput in the 60 GHz Band." *IEEE Standard 802.11ad*, 2012.

[17] W. Liu, F. Yeh, T. Wei, C. Chan, and S. Jou, "A Digital Golay-MPIC Time Domain Equalizer for SC/OFDM Dual-Modes at 60 GHz Band," *IEEE Transactions on Circuits and Systems I: Regular Papers*, vol. 60, no. 10, pp. 2730–2739, Oct 2013.

[18] H. Sawada, H. Nakase, S. Kato, M. Umehira, K. Sato, and H. Harada, "Impulse Response Model and Parameters for Indoor Channel Modeling at 60GHz," in *2010 IEEE 71st Vehicular Technology Conference*, May 2010, pp. 1–5.

[19] J. O. Lacruz, D. Juara, and J. Widmer, "Wideband Millimeter-Wave Open Experimentation Platform (Poster, peer-reviewed)," in *The Fifth Millimeter-Wave RCN Workshop*, Jan 2019.

[20] SIVERSIMA, *EVK06002 Development Kit*, accessed August 18, 2019, https://www.siversima.com/product/evk-600200.

[21] S. Sigg, M. Scholz, S. Shi, Y. Ji, and M. Beigl, "RF-Sensing of Activities from Non-Cooperative Subjects in Device-Free Recognition Systems Using Ambient and Local Signals," *IEEE Transactions on Mobile Computing*, vol. 13, no. 4, pp. 907–920, April 2014.

[22] S. Y. T. Yamawaki, "60-GHz Millimiter-Wave Automotive Radar," *Denso technical journal*, 1998.

[23] H. Hassanieh, O. Abari, M. Rodriguez, M. Abdelghany, D. Katabi, and P. Indyk, "Fast Millimeter Wave Beam Alignment," in *Proceedings of the 2018 Conference of the ACM Special Interest Group on Data Communication*, ser. SIGCOMM '18. New York, NY, USA: ACM, 2018, pp. 432–445.

[24] J. Palacios, P. Casari, H. Assasa, and J. Widmer, "LEAP: Location Estimation and Predictive Handover with Consumer-Grade mmWave Devices," in *IEEE INFOCOM 2019-IEEE Conference on Computer Communications*. IEEE, 2019, pp. 2377–2385.

[25] A. Loch, H. Assasa, J. Palacios, J. Widmer, H. Suys, and B. Debaillie, "Zero overhead device tracking in 60 ghz wireless networks using multi-lobe beam patterns," in *Proceedings of the 13th International Conference on emerging Networking EXperiments and Technologies*. ACM, 2017, pp. 224–237.

[26] I. Pefkianakis and K.-H. Kim, "Accurate 3d localization for 60 ghz networks," in *Proceedings of the 16th ACM Conference on Embedded Networked Sensor Systems*. ACM, 2018, pp. 120–131.

[27] S. Sur, I. Pefkianakis, X. Zhang, and K.-H. Kim, "Towards scalable and ubiquitous millimeter-wave wireless networks," in *Proceedings of the 24th Annual International Conference on Mobile Computing and Networking*. ACM, 2018, pp. 257–271.

[28] Z. Yang, P. H. Pathak, Y. Zeng, X. Liran, and P. Mohapatra, "Monitoring vital signs using millimeter wave," in *Proceedings of the 17th ACM International Symposium on Mobile Ad Hoc Networking and Computing*. ACM, 2016, pp. 211–220.